EMAS
Engineering Modelling, Analysis & Simulation
THE NAFEMS JOURNAL

NAFEMS
Vol. 4, Issue 1, 2027

Evaluating Packaging Sterilisation Efficacy Using Computational Fluid Dynamics

A. Basso[a,1], T. London[a], W. Pickles[a], Z. Bunner[b], T. Yunker[b], C. Perez[b] and M. Hutchinson[b]

[a]Reckitt Benckiser Health Care UK Ltd, Dansom Lane, Hull, HU8 7DS, United Kingdom
[b]Mead Johnson Nutrition, 2400 W Lloyd Expy, Evansville, IN 47712, United States

Abstract

Sterilisation of packaging with vapour hydrogen peroxide (VHP) is commonly used across the consumer-packaged goods (CPG), food, beverage, and pharmaceutical industries to prevent product contamination from bacteria, viruses and fungi, and for the removal of chemical residues and particulate matter. To verify the efficacy of sterilisation, experimental testing is undertaken whereby bacterial cultures are deposited prior to VHP exposure and then monitored to see if they remain and grow after VHP exposure. While this test indicates a pass or fail outcome, and where in the bottle the failure occurred, the test does not give insight into why the failure occurred. As companies increasingly aim to introduce more sustainable packaging concepts through lightweighting and geometry optimisation, understanding the "why" helps to assure safety and quality whilst accelerating the delivery of more sustainable packaging concepts to the consumer.

To that end, modelling and simulation serve as valuable tools to complement laboratory measurements, providing insights prior to physical testing. By understanding the flow of VHP during sterilisation and the concentration of VHP on the exposed surfaces, these techniques can provide greater confidence in the safety of the packaging. Moreover, with virtual Design of Experiments analysis, sensitivities to manufacturability tolerances can also be assessed.

The purpose of this study is to show how Computational Fluid Dynamics (CFD) can be used to achieve these objectives. To do so, this study compares typical and representative (but generic) bottle designs and processing conditions, highlighting differences in outcomes and complexities despite the geometric similarities. The differences are numerically quantified by calculating the Sterility Assurance Level (SAL) and other metrics from relevant CFD output variables. The following observations were made from the analyses: a) given fixed sterilisation processing conditions, the absolute dimensions of bottles and associated geometric features can significantly influence the transient flow during the bottle fill up process; b) the combined effects of the geometric features and the mass flow rate of VHP lead to non-negligible changes in VHP surface coverage which impact sterilisation efficacy. These observations can have a significant impact on products where the sterilisation processing conditions remain fixed but different bottle volumes (500mL, 1L, etc) are used.

Keywords

Bottle sterilisation, Computational Fluid Dynamics, Numerical Simulation, Sterility Assurance Level, Turbulent Mixing, Aseptic Filling, Packaging, Vapour Hydrogen Peroxide, VHP.

1 Introduction

Aseptic sterilisation of packaging is an essential process in the food, beverage, pharmaceutical, and consumer-packaged-goods (CPG) industries to assure quality and safety whilst enhancing product

[1]Corresponding author.
E-mail address: alessio.basso@reckitt.com (A. Basso)
https://doi.org/10.59972/4azftb9p

shelf life and durability. Various methods of sterilisation are used and have been studied over the years to determine the most effective ways to achieve micro-organism inactivation [1], as pathogens have the potential to cause severe side effects if not neutralised prior to ingestion [2], [3]. A typical sterilisation process consists of three different steps: a) pre-heating of packaging; b) injection of the sanitising mixture; and c) drying of the containers through dry, sterile, hot-air jets. Chemical sterilisation is the most common method across the CPG industry. Typically, vapour hydrogen peroxide (VHP) or liquid hydrogen peroxide (LHP) are used as sterilising agents, since they produce harmless by-products, such as oxygen and hydrogen. Due to the higher efficacy and processing speed compared to LHP, the VHP method is oftentimes preferred, relying on condensation as the primary mechanism for surface disinfection [4]. Once degradation of VHP has occurred, hydroxyl radicals are formed and act to produce a cellular damage to micro-organisms, through the rupture of their internal membrane [5]. This entire sequence relies on the condensation of VHP, which, in turn, is dependent on the input process parameters, such as concentration, temperature, and relative humidity.

Sterilisation processes face a few, non-trivial challenges. One of these is the sensitivity of packaging to the process jet temperatures, where plastic bottles can permanently deform and shrink under the effect of the thermal loads involved [6], [7]. On the other hand, the reach of the sterilising agent is not always possible at sufficient concentrations in some localised, high-curvature regions, such as bottle shoulders. Therefore, a practical process engineering challenge is to identify the optimal process parameters that can produce favourable momentum and mass transport of the sterilising agent towards the bottle surface. It is not just the localised geometric features which can impact sterilisation efficacy: absolute geometry (e.g. axial and volumetric dimensions) of packaging also influences the performance of sterilisation processes, especially, when the axial dimension of the bottle has an impact on the saturation and filling time. For these reasons, it is important to determine the most sensitive setup for each individual bottle design, which can contribute to optimising performance, efficiency, and efficacy of sterilisation [8], [9], [10]. On top of the above points, optimisation of sterilisation processes can contribute to a more sustainable process where less waste is produced [11], [12], [13].

Computational Fluid Dynamics (CFD) analysis is a valuable tool to understand sterilisation processes because it can reveal the detailed flow field and mass and heat transfer behaviour of VHP inside the packaging. In comparison with physical tests, which can only describe whether a bottle has passed or failed and provide the failure location, numerical analysis exposes the underlying flow behaviour, including recirculation and boundary layer separation. For packaging such as bottles, these detrimental flow behaviours often occur where surface curvature change is significant, for instance, shoulders and bottom corners.

The use of CFD to assess the efficacy and optimisation of cleaning processes like aseptic sterilisation, VHP sterilisation, and sanitisation of clean spaces have been extensively studied by several authors, [14]. For example, in [15] and [16] the authors predicted the inactivation of G. stearothermophilus spores in a sterilisation environment by developing a CFD model that included inactivation kinetics. Similar sterilisation studies have focused on steam sterilisation of cavities [17], aseptic jet penetration in vacuum and non-vacuum environments [18], and the prediction of the chemical response in steam sterilisation [19]. The authors of [20] built a multi-objective, optimisation model to verify the optimal process setup, particularly, the nozzle design and position for a sterilisation process involving spouted pouch packaging. Life cycle assessment based methods were also implemented by [21], as an alternative to CFD analysis, to determine the sterilisation performance of hot filling systems and aseptic PET bottle packaging. CFD simulations were also used to assess the performance of steam sterilisers for sanitisation of medical devices [22], with a particular focus on steam condensation across surfaces. CFD analysis was also implemented for high pressure thermal processing for commercial scale food sterilisation [23], where a CFD model was coupled with an Integrated Temperature Distributor to estimate the sterilisation efficacy, given a fixed thickness of the polymeric carrier. A comprehensive review of the use of CFD methods in thermo-chemical sterilisation was provided in [24].

The above literature predominantly focuses on the sterilisation process itself: how to identify the most appropriate process parameters given all other assumptions are fixed, or more generally, how to model the process. But, in industrial sterilisation processes, it is often not particularly feasible to adjust qualified process parameters every time that other features (like packaging geometry) change. Therefore, this gap in literature motivated the present study: to highlight how changes in geometry can significantly impact sterilisation efficacy, given fixed processing parameters, and what the key influence variables driving this change in efficacy are.

This study is intended as a methodology demonstration, rather than a comprehensive parametric study of sterilisation processes. To this end, two representative bottle geometries and a limited set of

operating conditions were selected to illustrate the sensitivity of sterilisation efficacy to geometric scaling and process variables. Consequently, the findings presented in this work should be interpreted as indicative rather than universally applicable design rules. The primary objective is to highlight the capability of CFD to provide insight into geometry–process interactions and to identify potential risk areas that may not be observable through experimental pass/fail testing alone.

The paper is structured in the following parts: Section 2 discusses the modelling setup, numerical approach and assumptions considered for analysis, including implemented verification and validation procedure; Section 3 provides a discussion on the main outcome and results from the numerical analysis, and the possible interpretations of data obtained from CFD computations; Section 4 is a summary of this work, providing recommendations and insights for further development.

2 Numerical Approach and Assumptions

2.1 Geometry

Two representative packaging concepts, namely an 8-ounce and a 32-ounce bottle, were chosen for this study. Bottle geometries and the overall simulation domain were built in Ansys SpaceClaim 2025 R1 software. The bottles under consideration are shown in Figure 1 and Figure 2 below. The bottles differ in their total volume, particularly, the main axial length and section profile. The axial profile is relevant with regards to variation of curvature at the top shoulder and bottom locations. These regions have an impact on susceptibility to flow separation and recirculation motions that prevent penetration of the sanitising agent down to the bottle surface.

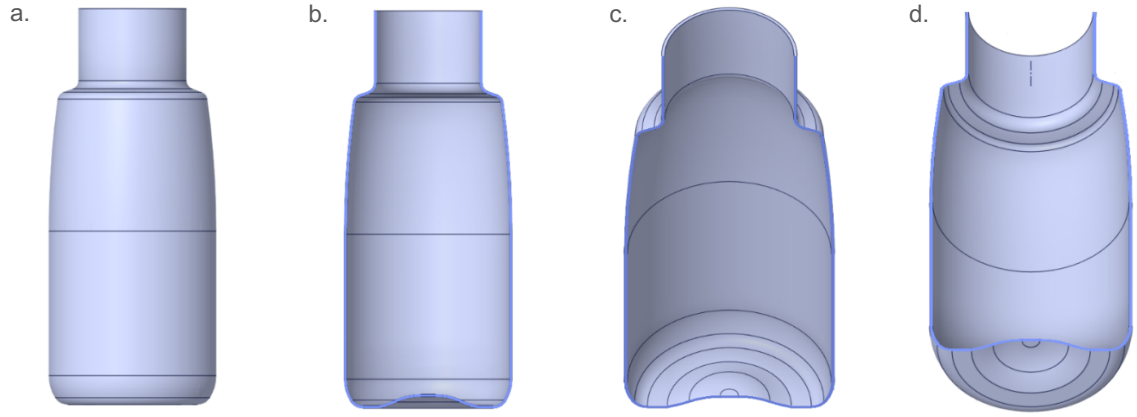

Figure 1.a. Generalised 8-ounce bottle design, side view, b. sliced side view, c. top-to-bottom sliced view, d. bottom-to-top sliced view.

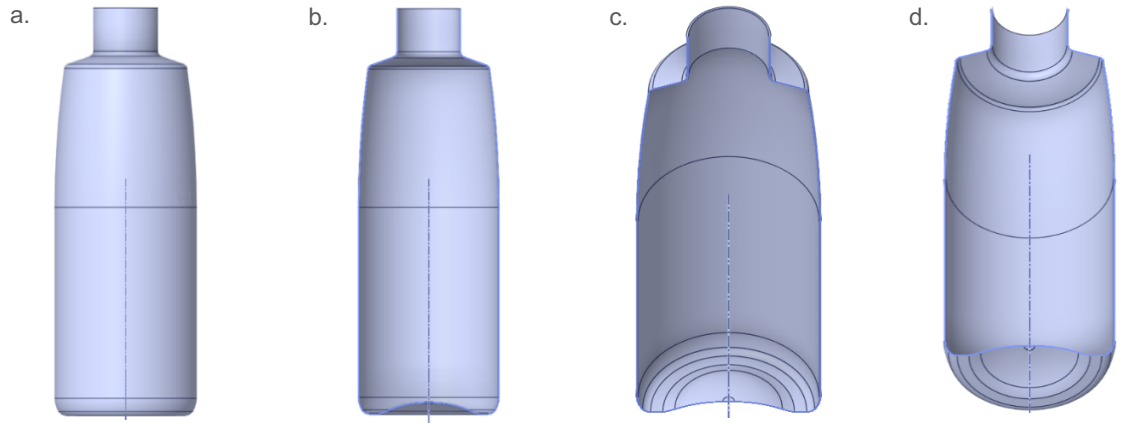

Figure 2.a. Generalised 32-ounce bottle design, side view, b. sliced side view, c. top-to-bottom sliced view, d. bottom-to-top sliced view.

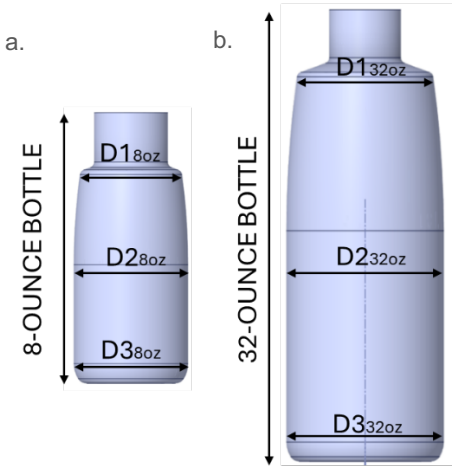

Figure 3.a. 8-ounce bottle dimensions design, b. 32-ounce bottle dimensions.

Geometrical ratios between the two bottle designs are summarised in Table 1 below.

Table 1. Geometrical ratios between bottle designs.

Ratio definition	Nomenclature	8-ounce bottle
Bottle Height Ratio	H_{8oz}/H_{32oz}	0.58
Top Shoulder Diameter Ratio	$D1_{8oz}/D1_{32oz}$	0.72
Mid-Section Diameter Ratio	$D2_{8oz}/D2_{32oz}$	0.70
Bottom Section Diameter Ratio	$D3_{8oz}/D3_{32oz}$	0.68

In terms of sterilisation setup, a conveyor belt system ensures that many bottles are sterilised simultaneously, by linearly translating under an array of sterilising jet nozzles, as illustrated in Figure 4.a. In this set up, a jet nozzle is positioned approximately 30 to 40 mm from each bottle top. The initial distance between a nozzle and the bottle axis along the travel direction was 50 mm.

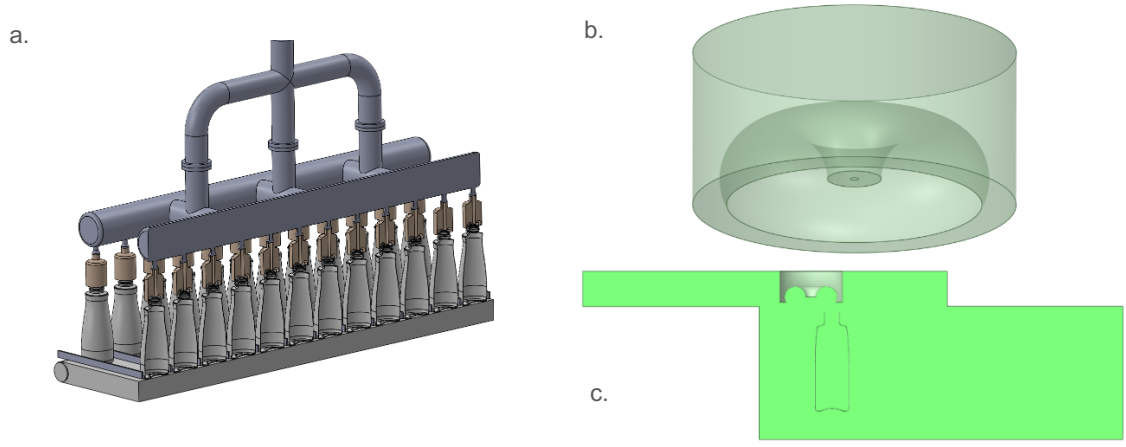

Figure 4.a. Schematic of a typical conveyor belt system, b zoom-in view of the injection system, c. numerical domain setup for CFD analysis of a single bottle.

2.2 Meshing Strategy

Due to the three-dimensional complexity of the bottles, unstructured, polyhedral meshes were adopted. Inflation layers were implemented on wall surfaces to produce reasonable velocity gradients in the wall-normal direction. The use of the Reynolds-Averaged-Navier-Stokes (RANS) method allowed the first-inflation layer thickness within the buffer region to have $y^+ \sim 30$. Ansys Fluent Meshing 2025 R1 software was used to generate meshes. A three-layered, smooth-transition inflation was applied to solid walls, with default settings for the boundary layer growth rate and the transition ratio. Local surface mesh size was set in the range 1.0-15.0mm. The maximum cell length was set to 25.0mm. Meshes are shown in Figure 5. to Figure 7.

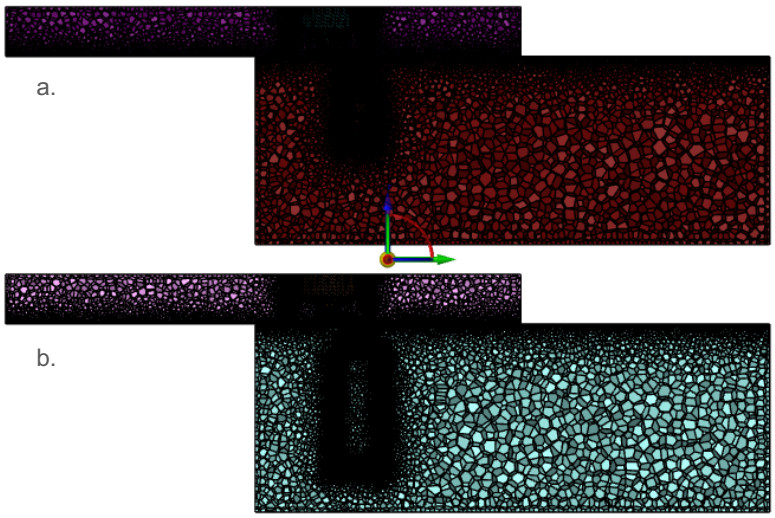

Figure 5.a Numerical domain mesh implemented in the current analysis for both 8-ounce bottle, and b. for 32-ounce bottle.

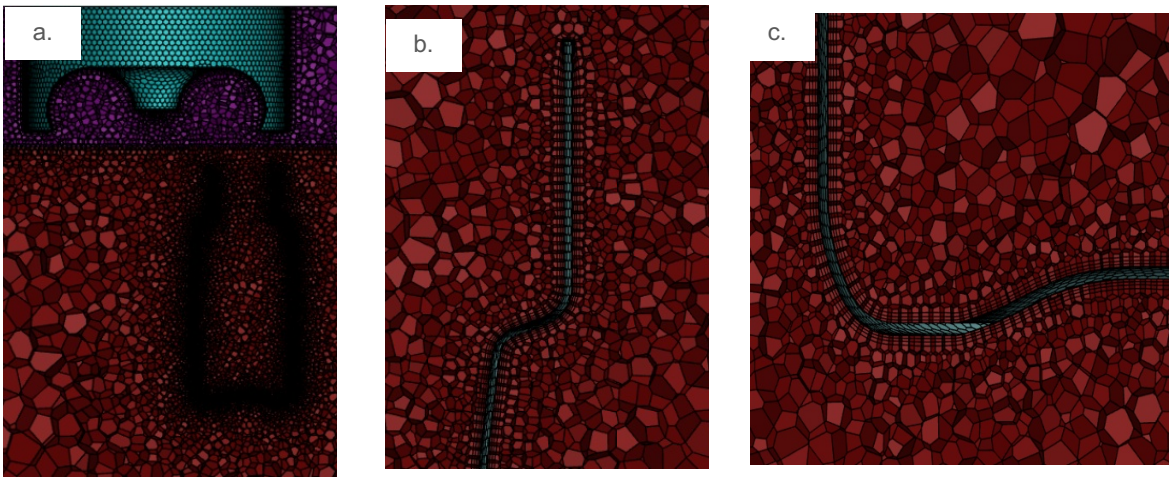

Figure 6.a. Polyhedral mesh implemented in the current analysis for the 8-ounce bottle, b. zoom-in view of the bottle shoulder, c. zoom-in of the bottom corner region.

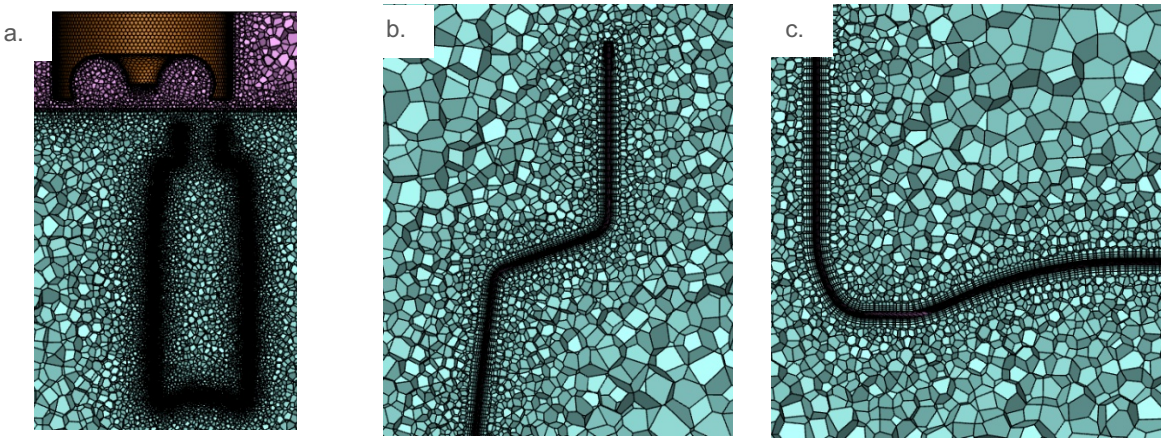

Figure 7. Polyhedral mesh implemented in the current analysis for the 32-ounce bottle, b. zoom-in view of the bottle shoulder, c. zoom-in of the bottom corner region.

2.3 Fluid Properties

The Species Transport model in Ansys Fluent was adopted to simulate the flow field and the transport of vapour hydrogen peroxide (VHP). This approach resolves the coupled conservation equations for mass, momentum, energy, and species concentration, enabling prediction of both fluid flow behaviour and species mixing within the domain.

Temperature-dependent properties for vapour hydrogen peroxide are shown in Table 2 and were sourced from [25]. The typical temperature range experienced in a sterilisation process is 40-120 ºC.

Table 2. Temperature-dependent properties of vapour hydrogen peroxide (VHP).

Operating temperature	Density	Specific Heat Capacity $x1.0^{+03}$	Thermal Conductivity $x1.0^{-02}$	Viscosity $x1.0^{-05}$	Diffusivity $x1.0^{-06}$
(ºC)	(kg/m^3)	(J/kg-K)	(W/m-K)	(kg/m·s)	(m^2/s)
40	1.39	1.55	2.6	0.99	6.72
60	1.38	1.60	2.7	1.06	7.48
80	1.37	1.65	2.8	1.13	8.29
100	1.36	1.70	2.9	1.20	9.13
120	1.35	1.75	3.0	1.27	10.00

An empirical correlation for the viscosity variation with respect to temperature of vapour hydrogen peroxide was suggested in [26], and provided below in Equation (1), where μ is the viscosity in micro poises, T is the mixture temperature in Celsius degrees and Y is the mole fraction (dimensionless) of hydrogen peroxide in the vapour phase:

$$\mu = 134 + 0.35 * (T - 100) - 14 * Y \quad (1)$$

In a typical sterilisation process, the concentration of hydrogen peroxide is within the range of 250 – 1,500 ppmv (parts per million by volume), corresponding to a mole fraction range of 2.5 x 10^{-4} - 1.5 x 10^{-3}, assuming ideal gas behaviour.

The variation of diffusivity with the operating temperature and pressure is often described by the Chapman-Enskog equation [27]. An approximate form of the Chapman-Enskog equation is often used in engineering applications where the full molecular detail is not required. In this way, the variation of diffusivity can simply be described by a general power law form, as in Equation (2) below:

$$D = D_0 \left(\frac{T}{T_0}\right)^n \quad (2)$$

In this study, the reference temperature T_0 was chosen equal to 120Cº, the diffusivity at the reference temperature D_0 was 1.0 x 10^{-5}cm^2/s, and the power-law exponent n was 1.75.

2.4 Boundary and Operating Conditions

The most relevant input parameters in a sterilisation process are a) the dwelling time, i.e. the period corresponding to the bottle being positioned underneath the sterilising nozzle; b) the mass flow rate of vapour hydrogen peroxide (VHP), which, given the fixed air flow, corresponds a fixed inlet VHP fraction in the sterilising mixture; c) the ambient (surrounding chamber) temperature; and d) the mixture stream or jet temperature. Table 3 below illustrates the sensitivity analysis undertaken in this study. In all cases, the mass flow of air, the operating temperature and pressure, and the temperature of the sterilising gas mixture were maintained constant, together with the bottle translation speed.

Table 3. Sensitivity study of a typical bottle sterilisation process.

Input parameter	Case 1	Case 2	Case 3	Case 4
Inlet mass flow – Air (SCFM)	50.0	50.0	50.0	50.0
Inlet mass flow – VHP (g/s)	2.0	2.0	0.5	0.5
Dwelling time (s)	3.0	5.0	3.0	5.0
Mixture jet temperature (ºC)	120.0	120.0	120.0	120.0
Operating temperature (ºC)	50.0	50.0	50.0	50.0

The conveyor belt setup, illustrated in Figure 4, was replicated in the numerical model. Bottles were initially set at a distance from the inlet nozzle, horizontally, of 50 mm.

The translational speed of bottles was set to 0.1 m/s instantaneously, therefore, there was no ramp up or ramp down of it. At time $t = 0.5$ s, bottle and nozzle axes are aligned. During the dwelling period, bottles stay stationary under nozzles.

Once the dwelling period has ended, bottles move away from nozzles at constant speed of 0.1m/s for 0.5 s. Therefore, the total simulation time was $t = 2 \times t_m + t_d$, where t_m is the relative motion period and t_d is the dwelling time. Simulation ends when the distance between bottle and nozzle is 50 mm.

The mass flow of the sterilising mixture was initiated at time $t = t_0 = 0.0$ s and stopped at the end of the dwell time for each case. These boundary conditions were set in the form of expressions in Ansys Fluent software. Default pressure outlet conditions were applied to the remaining boundary.

2.5 CFD Analysis Settings

A RANS, three-dimensional, transient, single-phase, non-reactive species transport model was built in Ansys Fluent software. This approach neglects phase change phenomena, particularly condensation of vapour hydrogen peroxide (VHP) on bottle surfaces, which is widely recognised as a primary mechanism driving microbial inactivation. Consequently, the results presented here should be interpreted as indicators of the transport and delivery potential of VHP rather than a direct prediction of disinfection kinetics. The focus of this work is on the macroscopic transport processes and their dependency on geometry and operating conditions. These simplifications, despite representing an important limitation, allow for a tractable and computationally efficient model.

The species transport model is used to model the mixing and transport of chemical species through solving the conservation equations for convection, diffusion, and reaction sources [28]. Therefore, it can be used in problems relating to species mixing with and without chemical reactions, or to model turbulent reacting flames. To predict the local mass fraction of each species (e.g. air and VHP), the convection-diffusion Equation (3) is resolved, where ρ is the mixture density, $\vec{v}$ is the velocity of the diffusing species, Y_i is the mass fraction of the i-th species, R_i is the net rate of production of the i-th species by chemical reaction [not applicable in the present case], J_i is the diffusion flux of the i-th species, and S_i is the rate of creation by addition from the dispersed phase and any other user-defined sources.

$$\frac{\partial}{\partial t}(\rho Y_i) + \nabla \cdot (\rho \vec{v} Y_i) = -\nabla \cdot \vec{J_i} + R_i + S_i \tag{3}$$

The diffusion flux term J_i, shown in Equation (4), is where the fluid properties of the mixture are included in the governing flow equation set:

$$\vec{J_i} = -\left(\rho D_{i,m} + \frac{\mu_t}{Sc_t}\right)\nabla Y_i \tag{4}$$

In laminar flows, Fick's law (dilute approximation) applies, meaning that mass diffusion is dominated by concentration gradients. In turbulent flows, the mass diffusion term has a turbulent contribution which is accounted through the turbulent Schmidt number ($Sc_t = \mu_t / \rho D_t$). The species transport model setup implemented in this analysis made use of the ideal gas mixing correlations to estimate density and viscosity of the mixture.

2.6 Verification and Validation

A mesh grid independence study was undertaken with respect to a) local mesh size on the bottle and nozzle surfaces; b) thickness of the first layer of boundary layer inflation across the same bottle and nozzle surfaces. Table 4 summarises the model setup for sensitivity with respect to the bottle surface size.

Table 4. Sensitivity study with respect to the mesh size on the bottle surface.

Dwelling time (s)	VHP flow rate *1.0e-03 (kg/s)	Number of inflation layers (-)	Surface mesh size – Bottle (mm)	Surface mesh size – Nozzle (mm)
1.0	2.0	3	7.50	2.5
1.0	2.0	3	3.75	2.5
1.0	2.0	3	1.50	2.5
1.0	2.0	3	1.25	2.5
1.0	2.0	3	1.00	2.5
1.0	2.0	3	0.75	2.5

The sensitivity study with respect to the mesh size on the bottle surface revealed an optimal size of approximately 1mm, leading to approximately 362,000 cells in the control grid. This corresponds to a variation in the residue value of VHP concentration of 0.28%. This outcome is visually represented in Figure 8.

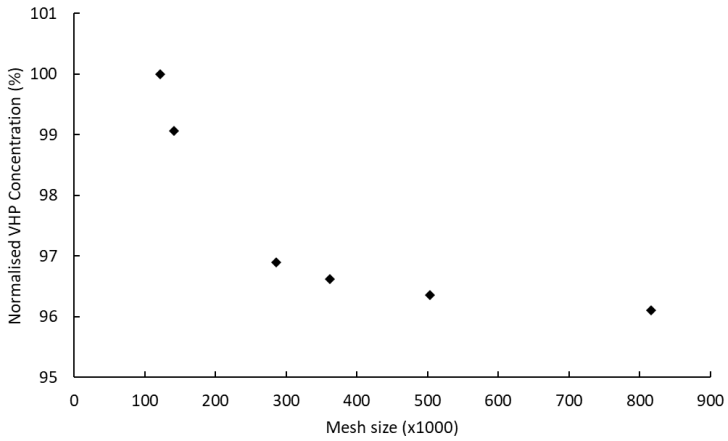

Figure 8. Mesh sensitivity with respect to mesh surface size on the bottle.

With regards to sensitivity with respect to the first-inflation thickness, the velocity profile in the wall-normal direction was analysed. A few considerations need to be made: 1) the flow field is dependent on heat fluxes and, subsequently, temperature variations; 2) the flow field is transitioning from a turbulent to a laminar regime and is not comparable to a conventional boundary layer flow, for instance in a pipe. The thickness of the first layer of inflation was set constant through the bottle surface. Values considered for this sensitivity are shown in Table 5.

Table 5. Sensitivity setup with respect to the thickness of the first inflation layer.

Vapour Temperature (ºC) (s)	Vapour Flow Rate (g/s)	Bottle Surface Size (mm)	Nozzle Surface Size (mm)	Thickness of First Inflation Layer (mm)
120	2.0	1.0	2.5	1.0
120	2.0	1.0	2.5	0.5
120	2.0	1.0	2.5	0.1

The following changes were implemented for the sensitivity model: a) a steady analysis applied to the 8-ounce bottle only; b) no sliding mesh or motion setup implemented, therefore, the nozzle was steadily positioned on top of the bottle. Profiles of velocity, normalised with the friction velocity, were calculated at two different wall locations and plotted with respect to the non-dimensional wall distance, $y^+ = u_* y/\nu$ in Figure 9. A friction coefficient of 0.005 was used to determine the friction velocity, as this is reasonably applicable to high-speed, compressible jets, such as in sterilisation.

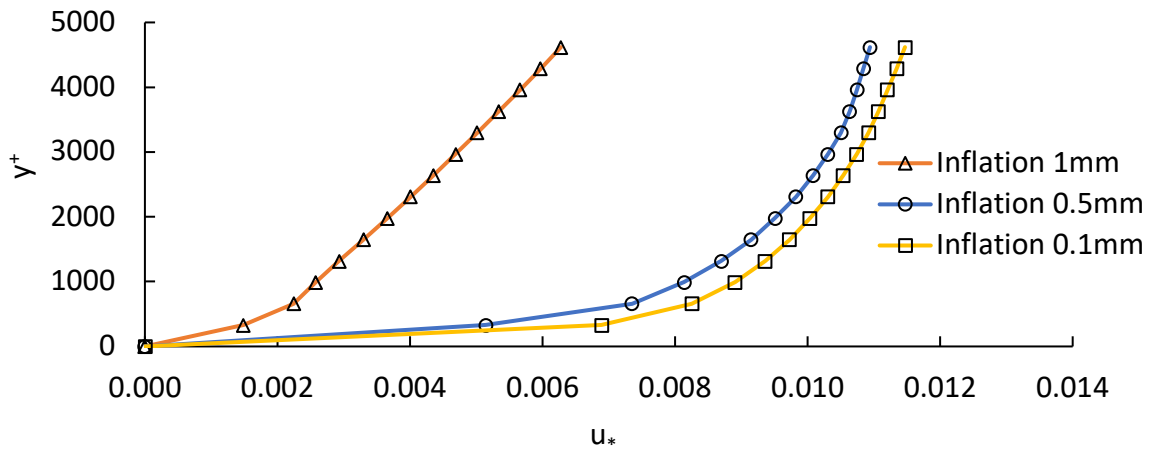

Figure 9. Mesh sensitivity with respect to mesh surface size on the bottle.

Results show that variations in velocity decrease as the inflation layer is compressed. Particularly, when the first inflation layer thickness goes from 1mm to 0.5mm, the minimum variation in u_* is in the order of 74%. However, when changing from a first inflation layer thickness of 0.5mm to 0.1mm, the minimum variation in u_* is in the order of 4%. These outcomes indicate that the RANS approach provided a reasonable compromise between solution accuracy and computational runtime.

Furthermore, while the numerical results provide detailed insight into flow and transport behaviour, it is important to acknowledge sources of uncertainty. A mesh sensitivity study indicated a variation of approximately 0.28% in the predicted VHP concentration, suggesting acceptable numerical convergence. However, additional uncertainties arise from modelling assumptions, including turbulence closure, boundary conditions, and the neglect of phase change and reaction effects. For this reason, the results are interpreted primarily in a relative sense, focusing on trends and comparative differences between geometries and operating conditions, rather than absolute quantitative predictions of sterilisation efficacy.

While direct quantitative validation against spatially resolved experimental measurements (for example, local VHP concentration fields or Particle Image Velocimetry flow visualisation) is not currently available, the present model was assessed through qualitative and physics-based validation considerations. The predicted flow structures, including jet impingement behaviour, recirculation zones, and progressive filling of confined geometries, are consistent with established fluid mechanics of turbulent jets interacting with enclosed cavities ([29], [30], [31]). Furthermore, the simulated trends—such as reduced sterilisation efficacy in larger bottles and in regions of high curvature (such as shoulders and bottom corners)—are consistent with empirical observations from industrial sterilisation testing, where failures are more likely in poorly ventilated or recirculating regions ([32], [33]).

2.7 Computational Resources

The typical mesh consisted of approximately 3.6×10^5 polyhedral cells, with transient RANS simulations performed using a pressure-based solver. Each transient CFD simulation required approximately 48 hours of wall-clock time using parallel computation on an Intel® Xeon® Gold 6240 CPU @ 2.60 GHz with 36 processing cores and 377 GB RAM. These computational requirements are considered manageable within an industrial workflow, particularly when compared to the time and cost associated with physical prototyping and testing. The approach is therefore well-suited for design screening and comparative studies, although large-scale parametric optimisation would benefit from further model reduction or high-performance computing resources.

3 Results and Discussion

3.1 Qualitative analysis of results

3.1.1 Overview

Numerical analysis is a useful tool to characterise the flow and heat transfer behaviour which otherwise would not be possible to characterise in the physical test environment. In comparison with using numerical modelling approach, physical testing will only tell whether packaging has passed the minimum sterilisation requirements. Physical testing does not specify the reasons why tests fail. For this reason, while physical testing provides confidence in the achieved outcome, simulations, even qualitative outcomes, provide insights necessary to improve the overall design process.

3.1.2 Flow field visualisation

Analysis of velocity contour plots on a section plane of the packaging can describe the local flow field distribution at locations where there is risk of ineffective sterilisation. From the fluid flow perspective, it is important that the sterilising agent can reach the surface of the bottle with sufficient concentration levels to be able to eliminate bacterial colonies. Therefore, it is important to analyse the regions subject to sudden change in curvature, where there is a high degree of flow recirculation and boundary layer separation.

Figure 10 shows in-plane components of vectors of velocity magnitude. Red colour corresponds to high velocity, whereas blue colour corresponds to low velocity. Vector arrows are scaled based on the magnitude of the local velocity field. Corner regions are those where there is likelihood of having bacterial contamination, therefore, where sterilisation will tend to fail. Because of the sudden change in

surface curvature, the boundary flow detaches in convex regions and reattach in concave areas. These sudden changes disrupt the diffusion of VHP across the near-wall region.

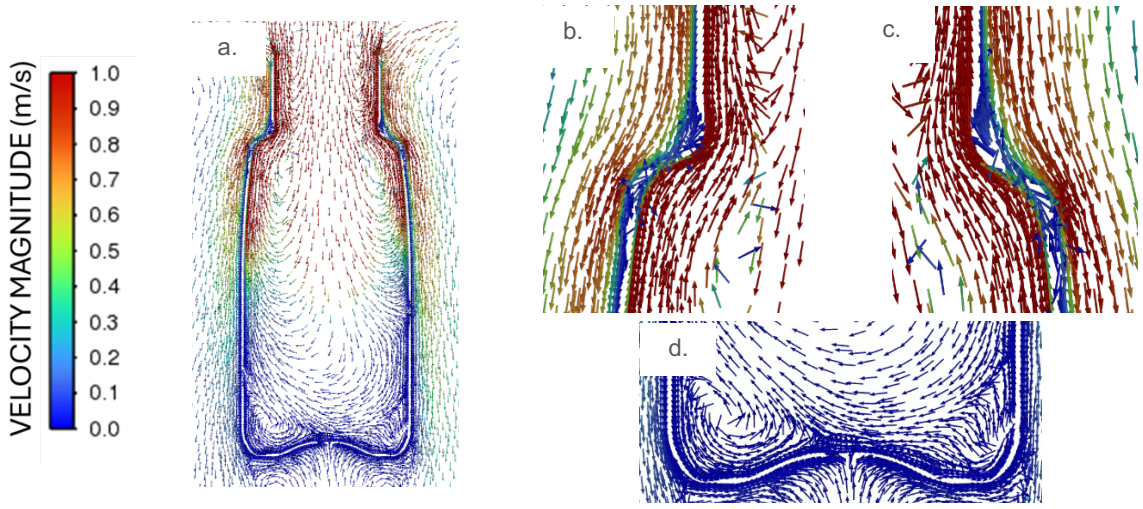

Figure 10.a. Velocity vector contours on the 8-ounce bottle, b. zoom-in view on the left shoulder, c. zoom-in view on the right shoulder of the bottle, d. zoom-in view of the bottom part of the bottle. Dwelling time: 3s; VHP mass flow: 0.5g/s.

An additional visualisation method is represented velocity path lines, which indicate the current trajectory of fluid particles within the enclosed geometry. In Figure 11 and Figure 12 velocity path line plots are shown for the 8-ounce and 32-ounce bottles at different time points. Images show that both bottle designs exhibit the same trend, i.e. the flow field transitions towards a laminar, ordered regime, due to the enclosed geometry of the bottle as time progresses. This process of laminarization takes a few seconds and correlates with the bottle VHP filling time.

Bottle filling and flow transition to laminar regime are affected by the bottle design, especially the axial dimension. In Figure 13 a snapshot of the VHP concentration contour is shown for the two bottle designs at 1.0s. It can be inferred that advection and diffusion play both a role in the bottle filling process. Flow advection is predominant in the early stages. However, as time passes and laminar transition has completed, diffusion becomes the predominant mechanism. When comparing the two bottles, the 8-ounce has filled more than the 32-ounce. By contrast, the 32-ounce bottle shows more significant concentration gradients, indicating that advection is still predominant over diffusion.

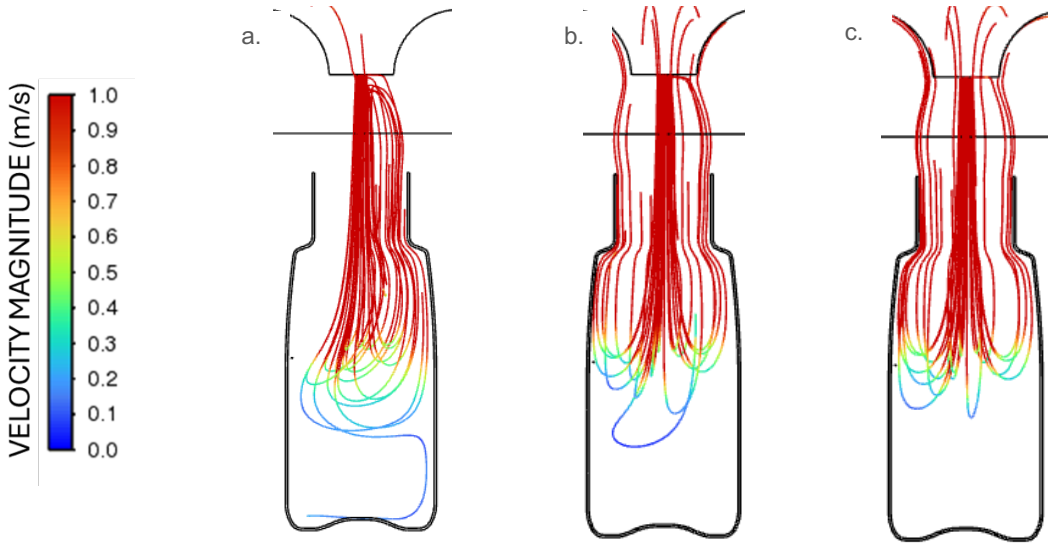

Figure 11.a. Velocity path line plots for the 8-ounce bottle at 1.0s, b. 2.0s, c. 3.0s. Dwelling time: 3s; VHP mass flow: 0.5g/s.

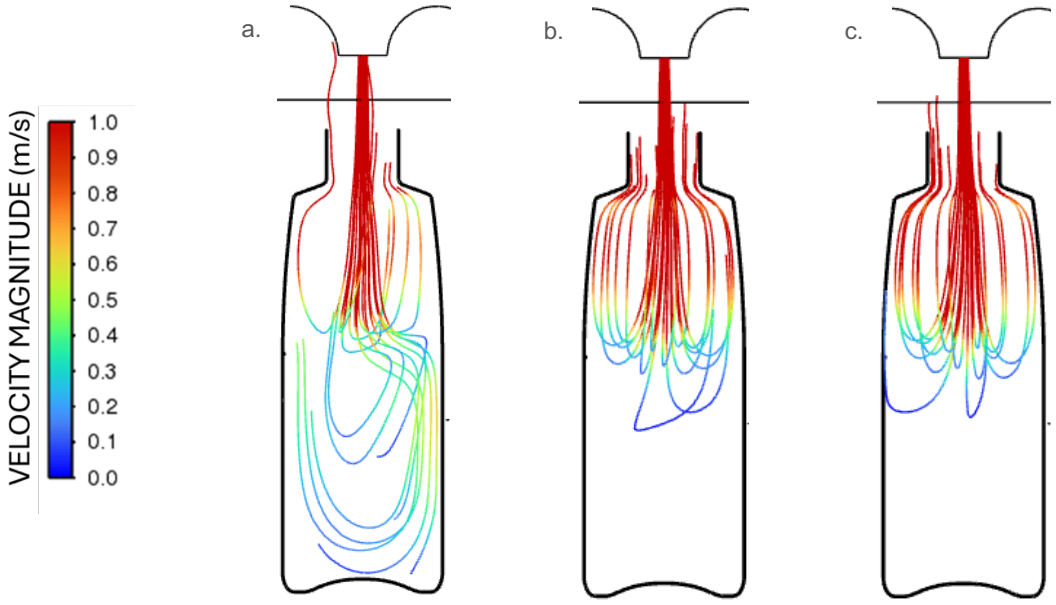

Figure 12.a. Velocity path line plots for a 32-ounce bottle at 1.0s, b. 2.0s, c. 3.0s. Dwelling time: 3s; VHP mass flow: 0.5g/s.

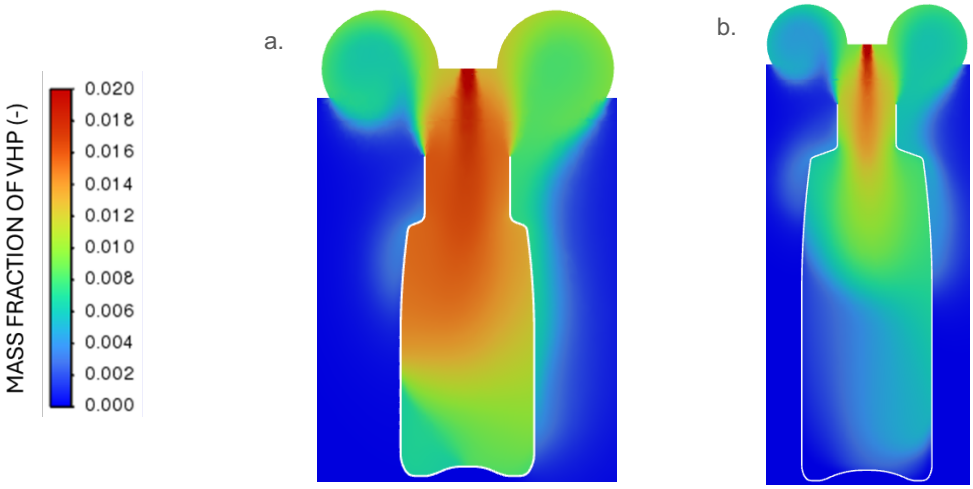

Figure 13.a. Contours of VHP concentration highlight the advection and diffusion mechanisms on the 8-ounce bottle, b. on the 32-ounce bottle at 1.0s. Dwelling time: 3s; VHP mass flow: 0.5g/s.

3.2 Quantitative analysis of results

3.2.1 Overview

This section provides quantitative results, particularly, transient concentration profiles of vapour hydrogen peroxide at 12 different point locations across the bottle surface. As illustrated in Figure 14, four locations were selected in the top shoulder, mid-waist and bottom regions, in the vicinity of corners, for a total of twelve points. Concentrations were averaged to simplify data output.

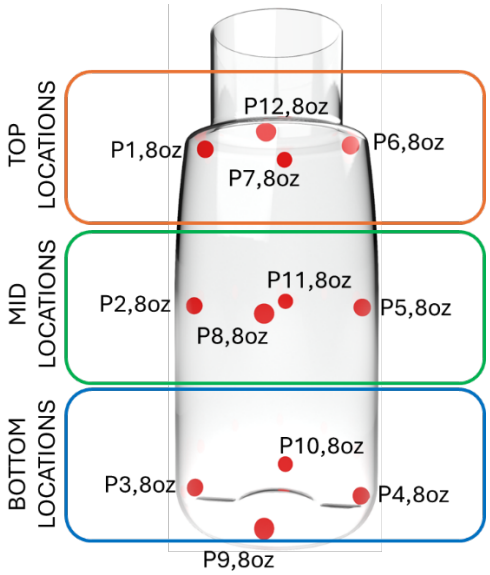

Figure 14. Illustration of point locations used to sample VHP concentration, 8-ounce bottle.

3.2.2 Transient concentration of vapour hydrogen peroxide

The dwelling time was defined in the previous sections as the process parameter where the bottle is in a fixed position with respect to the sterilising nozzle, coaxially with it. The dwelling time should not be confused with the filling time, which, instead, is a measure of the bottle volume being filled with the sterilising agent, when the average concentration in the bottle has reached saturation. In Figure 15, the transient average concentration of VHP is shown for top, mid and bottom locations, on the 8-ounce bottle, and for different dwelling periods. The following observations were made:

- Top and mid locations reach saturation approximately simultaneously, at around 3s from the process start. Bottom locations reach saturation later than the top and mid locations.
- The different dwelling times can be observed in each curve through the different time at which concentration of VHP is at the saturation point.
- If looking at the curve relating to the bottom location, when the dwelling time is 3 s, the bottle reaches a peak which is about at the saturation level. However, due to the shortness of the dwelling period, VHP concentration drops afterwards.
- When considering different dwelling times, there is no difference between dwelling time of 3s and 5s in terms of VHP saturation value, regardless of the location.

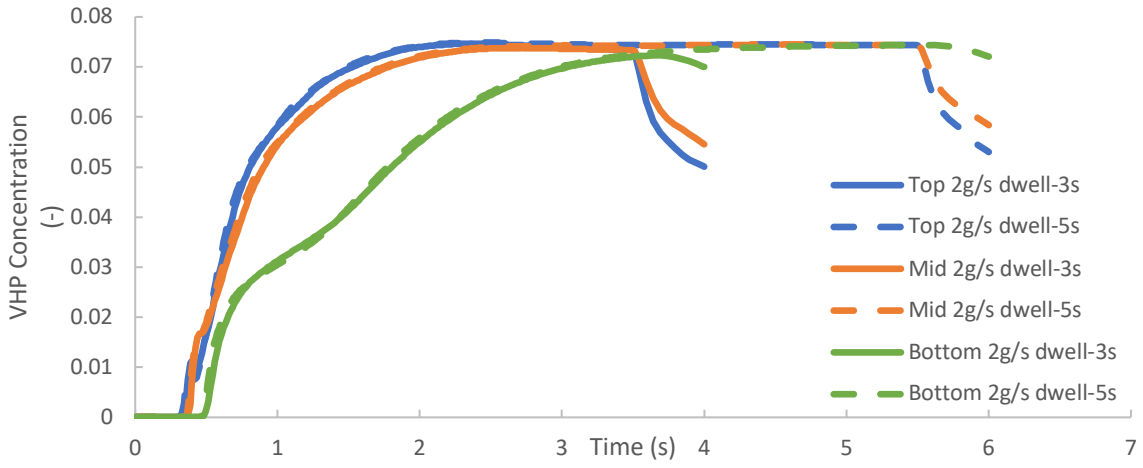

Figure 15. Transient profiles of VHP concentration versus dwelling time. Mass flow of VHP fixed at 2.0g/s, 8-ounce bottle.

When considering the same plot as in Figure 15, applied to the 32-ounce bottle, the axial dimension of the packaging has changed. The axial dimension influences the overall VHP concentration. Figure 16

below shows that, for all cases, except the top location with dwelling time of 3s, saturation is not reached on the 32-ounce bottle, regardless of the dwelling time.

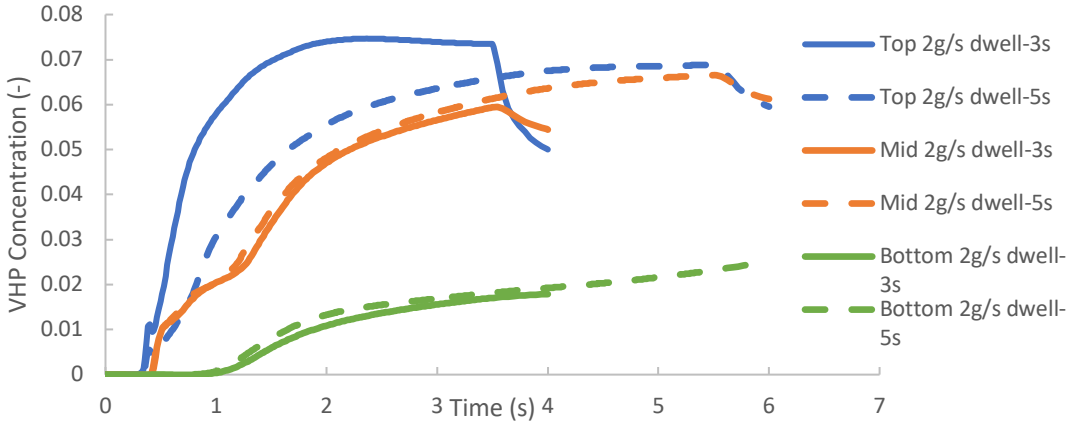

Figure 16. Transient profiles of VHP concentration versus dwelling time. Mass flow of VHP fixed at 2.0g/s, 32-ounce bottle.

As highlighted in Section 3.1, it takes some time to reach saturation condition. During this transient period, advection phenomena are predominant over diffusion, as the flow is chaotic and turbulent while the bottle is being filled. In the 32-ounce bottle, data suggest that, within the dwelling time, the flow regime is still transitional. This outcome might explain the difference with Figure 15.

A different trend was observed when varying the mass flow. Figure 17 and Figure 18 show that the saturation level changes significantly with the mass flow of VHP, regardless of the surface location.

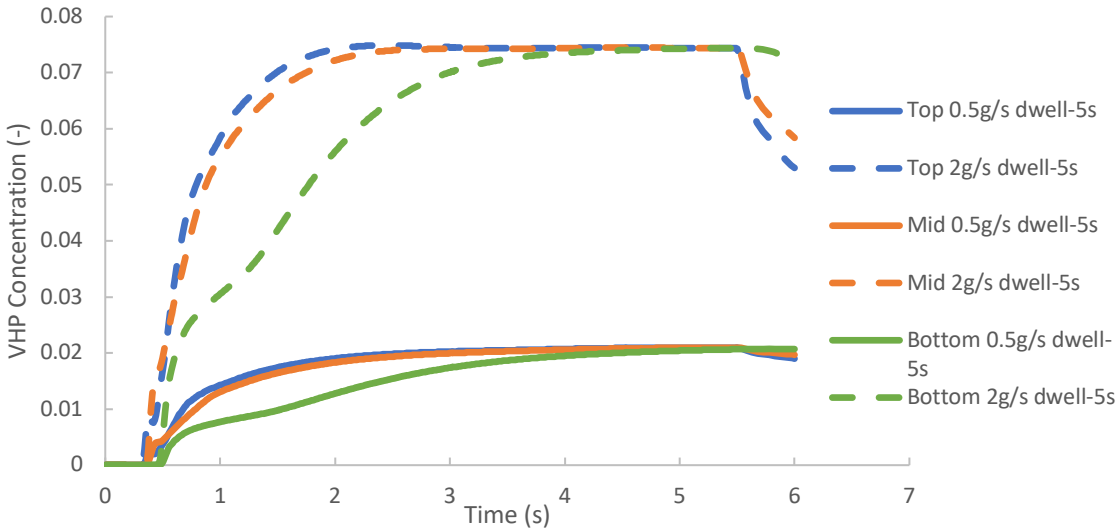

Figure 17. Transient profiles of VHP concentration versus mass flow. Dwelling time fixed at 5s, 8-ounce bottle.

For the 32-ounce bottle, saturation condition was not reached, leading the flow field to be still chaotic and flow advection effects being predominant over diffusion.

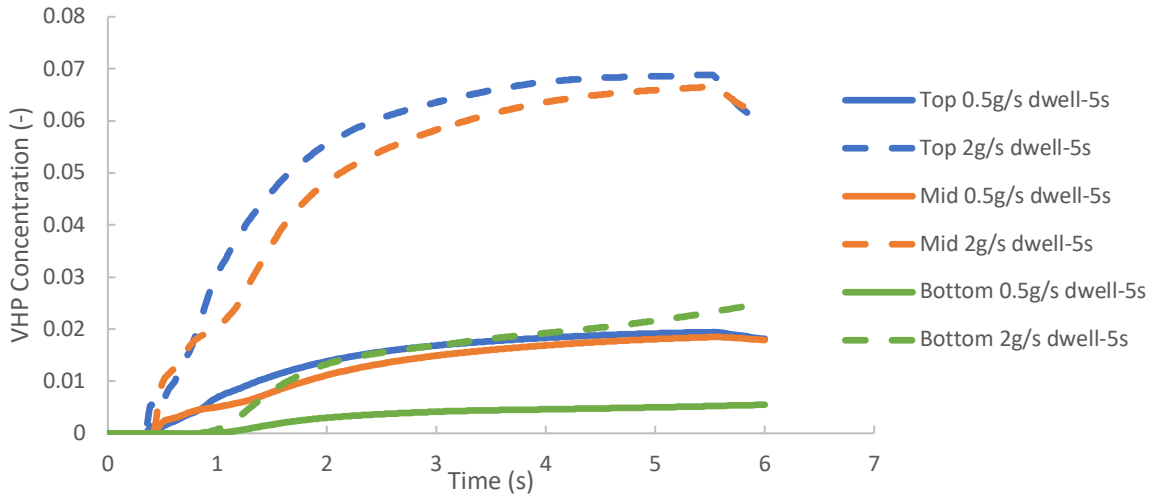

Figure 18. Transient profiles of VHP concentration versus mass flow. Dwelling time fixed at 5s, 32-ounce bottle.

3.2.3 Sterility Assurance Level (SAL)

Sterility Assurance Level (SAL) is a measure of the efficacy of sterilisation processes. SAL is defined, through Equation (5), as the probability of a single micro-organism surviving on a product surface after sterilisation has taken place.

$$SAL = 10^{-log_{10}\left(\frac{N_0}{N}\right)} \tag{5}$$

In Equation (5), N_0 and N are respectively the microbial load prior and after sterilisation has taken place. The whole argument of the 10-th power function is called Logarithmic Reduction Value (LRV) and is an important parameter to consider when it comes to distinguishing between different levels of sterilisation. Depending on the application, there are different levels of allowable contamination (

Table 6, [29]).

Table 6. Typical Sterility Assurance Level values in various CPG contexts and applications.

SAL value	Probability of Contamination	Typical Use Cases
10^{-3}	1 in 1,000	Products in contact with non-sterile surfaces (topical creams, household cleaning products).
10^{-5}	1 in 100,000	High-risk items where products might not tolerate harsher sterilisation environments.
10^{-6}	1 in 1,000,000	Products entering the body areas (injectable, surgical dressings, sterile drug packaging).

In a physical test environment, the SAL values can be directly measured through the microbial load on a test surface, prior to and after sterilisation. However, when dealing with CFD analysis and modelling, the process is as follows. Firstly, the transient concentration profiles of VHP are evaluated; the second step is to determine the total exposure of VHP concentration. This is the time integral of the VHP transient concentration versus time. Thirdly, the Desired Reduction value, or D-value should be determined. The D-value is defined as the time or period, measurable in seconds, leading to a reference 90% reduction (one log reduction) of microbial load, during sterilisation. The D-value is a known empirical quantity and is dependent on the specific microbial organism, as different micro-organisms have varying levels of resistance to sterilisation due to differences in their structure, physiology and protective mechanisms. The fourth step is to determine the Logarithmic Reduction Value (LRV), as the ratio between the total exposure, determined from CFD data, and the D-value:

$$LRV = \frac{1}{D}\frac{\int_{t0}^{t1} C(t)dt}{\int_{t0}^{t1} dt} \tag{6}$$

The Sterility Assurance Level value (SAL) is the final step in the calculation:

$$SAL = 10^{-LRV} \tag{7}$$

Note that a lower SAL values means a lower probability of contamination, therefore, better sterilisation.

Figure 19 and Figure 20 show the SAL value at the previously described 12 locations across the 8-ounce bottle surface, where variations were measured for different dwelling times and mass flows. Adjacent pairs of bars correspond to the same location but a numerical parameter being changed. Results indicated the following trends:

- In Figure 19, a larger dwelling time leads to better sterilisation efficacy, as the sterilising agent has more time to penetrate the bottle boundary layer down to the solid wall.
- In Figure 20, a larger mass flow of VHP results in lower SAL values, hence better sterilisation performance.
- Generally, as shown in Figure 21 for the case of 0.5g/s and 3s dwell, the studied sterilisation parameters work better for the 8-ounce bottle than the 32-ounce. This is because the 8-ounce bottle has fully transitioned to laminar flow and diffusion-dominated phenomena. By contrast, due to the large axial size, the 32-ounce bottle shows the advective flow mechanisms still conflicting with diffusion.

When interpreting SAL results, it is useful to consider typical industry benchmarks. For many consumer-packaged goods applications, acceptable SAL values range between 10^{-3} and 10^{-6}, depending on product risk classification. The present results indicate that, under fixed process conditions, smaller geometries (e.g., 8-ounce bottles) more readily achieve lower SAL values, whereas larger geometries may struggle to reach equivalent levels within the same dwelling time.

From a practical perspective, this suggests that maintaining sterilisation performance across different packaging sizes may require adjustments to key process parameters, such as increasing VHP mass flow rate or extending dwelling time. These findings highlight the importance of considering geometry-process interactions during design and scale-up.

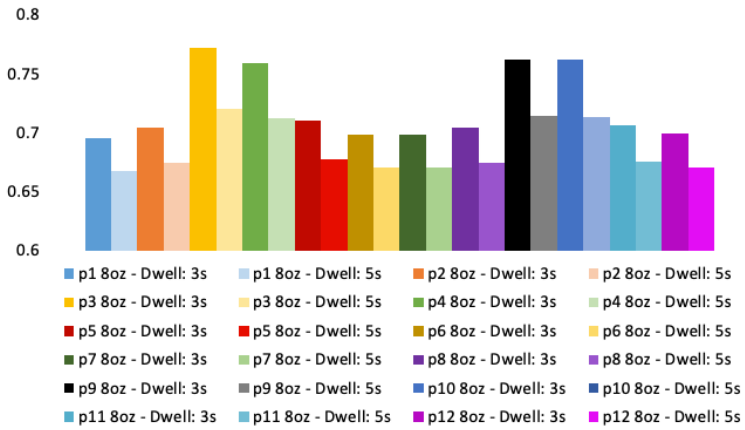

Figure 19. Sterility assurance level variation with respect to the dwelling time, at 12 different point locations on the 8-ounce bottle. VHP Mass flow equal to 0.5g/s.

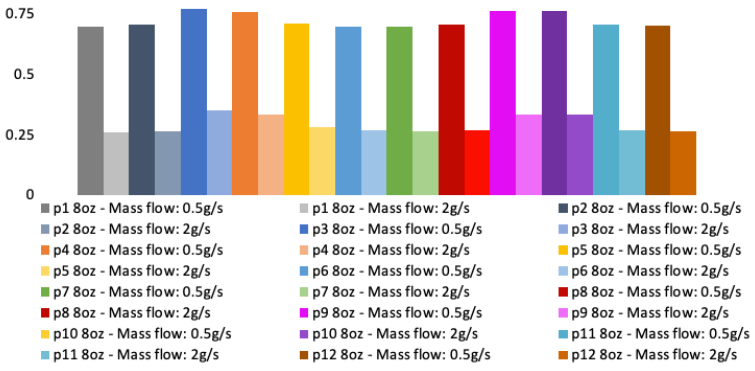

Figure 20. Sterility assurance level variation with respect to the mass flow, at 12 different point locations on the 8-ounce bottle. Dwelling time is 3.0s.

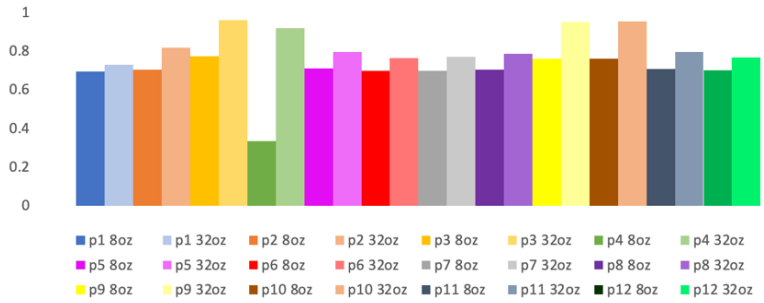

Figure 21. Sterility assurance level variation with respect to the geometries (8-ounce vs. 32-ounce bottles), at 12 different point locations. Dwelling time is 3.0s and mass flow of VHP is 0.5g/s.

4 Conclusions

This work has focused on identifying and emphasising how both the packaging geometry and the sterilisation processing conditions impact sterilisation efficacy. Analyses indicated the following trends:

- Qualitative analysis of the flow field indicated that the regions where geometry curvature changes rapidly are likely to be at risk of contamination, due to flow separation and recirculation, preventing access of VHP to effectively sanitise the wall.
- Path line plots showed that the flow regime move from a turbulent state, where flow advection dominates over diffusion, into laminar flow, where diffusion dominates. Ensuring sufficient processing time is available to achieve the diffusion-dominant regime is essential for sterilisation efficacy.
- Where the findings impact the real-world is that oftentimes the same product is sold in different packaging sizes (e.g. 8oz and 32oz). In this case, where qualified process parameters may not be readily modified, CFD provides insight into the risks that different design changes may present.
- Transient profiles of VHP concentration indicated that the saturation level much more significantly influenced by mass flow rate of VHP rather than dwell time. Therefore, mass flow of VHP is a crucial parameter to optimise or to improve the sterilisation process.
- The same trends were confirmed by plots of SAL values, where the sterilisation efficacy increases with the dwelling time and the mass flow of VHP. Furthermore, comparing the 8-ounce and 32-ounce bottles, the 8-ounce bottle has better SAL values than the 32-ounce bottle, which can be presumably explained with the condition of saturation being reached, hence, diffusion effects becoming predominant on flow convection.

While the specific examples highlighted in this work are representative and indicative of geometries and processing conditions used in industry, the results should be considered cautiously due to the narrow range of solution variations considered within the sensitivity study. That said, the results emphasise the significant role that CFD and simulation can play in accelerating product development timelines both with respect to more sustainable packaging concepts and quality. Simulation can provide insights on why alternative packaging designs may pass or fail sterilisation. This methodology has the potential to reduce unnecessary delays and costs related to physical testing and manufacturing. As companies increasingly aim to introduce more sustainable packaging concepts through lightweighting and geometry optimisation, understanding the "why" helps to assure safety and quality whilst accelerating the delivery of more sustainable packaging concepts to the consumer.

Future work will focus on extending the present methodology in several key directions. Firstly, the incorporation of multiphase modelling, including VHP condensation and surface interaction, will enable a more realistic representation of sterilisation mechanisms. Secondly, targeted experimental validation campaigns, including measurements of concentration fields and microbial inactivation, will be pursued to further strengthen model credibility.

In addition, expanding the parameter space to include a wider range of geometries and operating conditions will support the development of generalised design guidelines. Finally, integration of CFD-based insights into digital engineering workflows and quality control frameworks represents a promising opportunity to accelerate decision-making in packaging development.

5 Nomenclature

5.1 Acronyms

CFD	Computational Fluid Dynamics
CPG	Consumer-Packaged Goods
LHP	Liquid Hydrogen Peroxide
LRV	Logarithmic Reduction Value
PET	Polyethylene Terephthalate
ppmv	Parts per million by volume
RANS	Reynolds-Averaged Navier-Stokes
SAL	Sterility Assurance Level (-)
SCFM	Standard Cubic Feet per Minute
VHP	Vapour Hydrogen Peroxide

5.2 Roman symbols

C	VHP concentration (-)
C(t)	Time-dependent VHP concentration (-)
D	Diffusivity (m²/s)
D_0	Reference diffusivity (m²/s)
D-value	Time for one-log (90%) microbial reduction (s)
D_t	Turbulent mass diffusivity (m²/s)
H	Bottle height (m)
J_i	Diffusion flux of species I (kg/ m²·s)
N	Microbial load after sterilisation (-)
N_0	Initial microbial load before sterilisation (-)
n	Power-law exponent for diffusivity correlation (-)
R_i	Net species production rate (kg/m^3·s)
S_i	User-defined source term (kg/m^3·s)
t	Time (s)
t_d	Dwelling time (s)
t_m	Relative motion period (s)
T	Temperature (ºC)
T_0	Reference temperature (ºC)
u_*	Friction velocity (m/s)
v	Velocity vector (m/s)
Y	Mole fraction of VHP (-)
Y_i	Mass fraction of species i (-)
y	Wall-normal distance
y^+	Non-dimensional wall distance (-)

5.3 Greek symbols

∇	Gradient/divergence symbol
$\partial/\partial t$	Temporal derivative operator
μ	Dynamic viscosity (Pa·s)
μ_t	Turbulent viscosity (Pa·s)
ν	Kinematic viscosity (m²/s)
ρ	Density (kg/m³)

5.4 Dimensionless numbers

Sc_t	Turbulent Schmidt number
H_{8oz}/H_{32oz}	Bottle height ratio
$D_{1\,8oz}/D_{1\,32oz}$	Top shoulder diameter ratio
$D_{2\,8oz}/D_{2\,32oz}$	Mid-section diameter ratio
$D_{3\,8oz}/D_{3\,32oz}$	Bottom-section diameter ratio

6 References

[1] A. Ansari, “An Overview of Sterilization Methods for Packaging Materials Used in Aseptic Packaging Systems,” Food and Bioproducts Processing, vol. 81, no. 1, pp. 57-65, 2003.

[2] “Principles of Food Safety and Quality Management - Common Biological Hazards in Food Safety,” Food Safety Institute, January 2004. [Online]. Available: https://foodsafety.institute/fqs-principles-mgt/common-biological-hazards-food-safety/#google_vignette.

[3] A. Akinsemolu and H. Onyeaka, “Microorganisms Associated with Food Spoilage and Foodborne Diseases,” Food Safety and Quality in the Global South, pp. 489-531, August 2024.

[4] K. Leonie, J. Rauschnabel and H. Langowski, “Influencing parameters of vaporized hydrogen peroxide on the sterilization of polyethylene terephthalate bottles,” Food Packaging and Shelf Life, vol. 36, no. 101053, April 2023.

[5] P. Setlow, “Resistance of Bacterial Spores,” in Bacterial Stress Responses, Second Edition, 2010.

[6] P. Kirchner, J. Oberländer, H. Suso, G. Rysstad, M. Keusgen and M. Schöning, “Monitoring the microbicidal effectiveness of gaseous hydrogen peroxide in sterilisation processes by means of a calorimetric gas sensor,” Food Control, vol. 31, no. 2, pp. 530-538, 2013.

[7] S. Reisert, H. Geissler, C. Weiler, P. Wagner and M. Schöning, “Multiple sensor-type system for monitoring the microbicidal effectiveness of aseptic sterilisation processes,” Food Control, vol. 47, pp. 615-622, 2015.

[8] H. Weisser and M. Zuber, “Aseptic Filling of Beverages in Glass Bottles - New Developed Processes in Germany,” Developments in Food Engineering., pp. 802-804, 1994.

[9] Z. Jildeh, P. Wagner and M. Shoning, “Sterilisation of Objects, Products, and Packaging Surfaces and Their Characterisation in Different Fields of Industry: The Status in 2020,” Physica Status Solidi, vol. 218, pp. 1-27, 2021.

[10] B. Verjans, “Challenges and Innovation in Aseptic Filling: Case Study with the Closed Vial Technology,” in AAPS Advances in the Pharmaceutical Science Series - Sterile Product Development, New York, NY, Springer, 2013, pp. 249-274.

[11] T. Sandle, “An Anatomy of a Contamination Control Strategy for Sterile Manufacturing,” Journal of GxP Compliance, vol. 25, no. 2, March 2021.

[12] Y. Patel and V. Patel, “11 Key Contributing Factors for Maintaining Sterility Assurance,” Pharmaceutical Online, 6 January 2025. [Online]. Available: https://www.pharmaceuticalonline.com/doc/11-key-contributing-factors-for-maintaining-sterility-assurance-0001.

[13] S. Chakraborty; H. Baseman, “Contamination Control Strategies: A Path for Quality & Safety,” Gxpfont Consulting Group; ValSource, Inc, 18 May 2022. [Online]. Available: https://www.pda.org/pda-letter-portal/home/full-article/contamination-control-strategies-a-path-for-quality-safety.

[14] A. Jung and P. Fryer, “Optimising the quality of safe food: Computational modelling of a continuous sterilisation process,” Chemical Engineering Science, vol. 54, no. 6, pp. 717-730, 1999.

[15] M. Feurhuber, R. Neuschwander, T. Taupitz, V. Schwarz, F. Carsten and C. Hochenauer, “A Computational Fluid Dynamics (CFD) model to simulate the inactivation of Geobacillus stearothermophilus spores in different moist heat sterilization environments,” Physics in Medicine, vol. 12, no. 100039, 2021.

[16] M. Feurhuber, A. Cattide, M. Magno, M. Miranda, R. Prieler and C. Hochenauer, “Prediction of the fluid flow, heat transfer and inactivation of microorganism at medical devices in modern steam sterilizers using computational fluid dynamics,” Applied Thermal Engineering, vol. 127, pp. 1391-1403, 2017.

[17] M. Feurhuber, M. Magno, M. Miranda and C. Hochenauer, “CFD investigations of steam penetration, air-removal and condensation inside hollow loads and cavities,” Appl. Therm. Eng., vol. 147, pp. 1070-1082, 2019.

[18] M. Feurhuber, M. Magno, M. Miranda, R. Prieler and C. Hochenauer, “CFD investigation of non-condensable gases in vacuum and non-vacuum steam sterilizers,” Chem. Ing. Tech., vol. 91, pp. 1-13, 2019.

[19] P. Burian, M. Feurhuber, M. Miranda, M. Magno and C. Hochenauer, “Numerical prediction of the chemical indicator response used in steam sterilisers,” Phys. Med., no. 1000034, 2020.

[20] S. Spanu and G. Vignali, “Modelling and Multi-objective Optimisation of the VHP Pouch Packaging Sterilisation Process,” International Journal of Food Engineering, vol. 12, no. 8, 2016.

[21] G. V. M. Manfredi, “Comparative Life Cycle Assessment of hot filling and aseptic packaging systems used for beverages,” Journal of Food Engineering, vol. 147, pp. 39-48, 2015.

[22] M. Feurhuber, A. Cattide, M. Magno, M. Miranda, R. Prieler and C. Hochenauer, “Prediction of the fluid flow, heat transfer and inactivation of microorganism at medical devices in modern steam sterilizers using computational fluid dynamics,” Applied Thermal Engineering, vol. 127, pp. 1391-1403, 2017.

[23] K. Knoerzer, R. Buckow, B. Chapman, P. Juliano and C. Versteeg, “Carrier optimisation in a pilot-scale high pressure sterilisation plant – An iterative CFD approach employing an integrated temperature distributor (ITD),” Journal of Food Engineering, vol. 97, no. 2, pp. 199-207, 2010.

[24] B. Y. H. Park, “Computational Fluid Dynamics (CFD) Modelling and Application for Sterilization of Foods: A Review,” Processes, vol. 6, no. 62, 2018.

[25] M. Sawale, A. Singh, P. Benyathiar, F. Ozadali, A. Bhunia and V. Pol, “Inactivation kinetic parameters of hydrogen peroxide application in commercial sterility of aseptic processing systems,” Journal of Food Engineering, vol. 378, 2024.

[26] C. Satterfield, “The Viscosity of Vapor Mixtures of Hydrogen Peroxide and Water,” in D.I.C 6552, Report No. 39, 1953.

[27] Mason and Marrero, “Gaseous Diffusion Coefficients,” Journal of Physical and Chemical Reference Data, vol. 1, no. 3, 1972.

[28] “Species Transport and Finite Rate Chemistry,” in Ansys Fluent 2025 R2 - Theory Manual.

[29] U. F. &. D. Administration, “Sterilization Process Controls,” [Online]. Available: https://www.fda.gov/inspections-compliance-enforcement-and-criminal-investigations/inspection-guides/sterilization-process-controls. [Accessed 20 February 2026].

[30] “Ensuring Compliance and Competitiveness: The Critical Role of Food Safety and Transparency in the CPG Industry,” Movista - Industry Insights, [Online]. Available: https://explore.movista.com/blog/ensuring-compliance-and-competitiveness-the-critical-role-of-food-safety-and-transparency-in-the-cpg-industry. [Accessed May 2025].

[31] T. Bassett, B. Viggiano, T. Barois, M. Gibert, N. Mordant, R. Cal, R. Volk and M. Bourgoin, “Entrainment, diffusion and effective compressibility in a self-similar turbulent jet,” Journal of Fluid Mechanics, vol. 947, pp. A29-1 - A29-30, 2022.

[32] H. Dannbauer, M. Meise, O. Gattringer and M. Steinbatz, “Integrating Virtual Test Methods and Physical Testing to Assure and Reduce Effort and Time,” SAE 2006 Commercial Vehicle Engineering Congress & Exhibition, 2006.

[33] L. Grealou, Driving CPG and FMCG Product Quality, Compliance, Consumer Trust, and Brand Reputation, Aras: 25 Years id Innovation and Growth, 2024.

[34] W. Lau, J. Reizes, V. Timchenko, S. Kara and B. Kornfeld, “Numerical modelling of an industrial steam–air sterilisation process with experimental validation,” Applied Thermal Engineering, vol. 75, pp. 122-134, 2015.

[35] M. Narayanan and A. Banerjee, “Computer Aided Analysis, Simulation and Optimisation of Thermal Sterilisation Processes,” Recent Patents on Biotechnology, vol. 7, no. 1, pp. 47-60, 2013.